Journal of Quantitative Spectroscopy & Radiative Transfer 112 (2011) 937–951

Contents lists available at ScienceDirect

Journal of Quantitative Spectroscopy & Radiative Transfer

journal homepage: www.elsevier.com/locate/jqsrt

The 1.58 μm transparency window of methane (6165–6750 cm^{-1}): Empirical line list and temperature dependence between 80 and 296 K

L. Wang [a], S. Kassi [a], A.W. Liu [a,b], S.M. Hu [b], A. Campargue [a,*]

[a] Laboratoire de Spectrométrie Physique (associated with CNRS, UMR 5588), Université Joseph Fourier de Grenoble, B.P. 87, 38402 Saint-Martin-d'Hères Cedex, France

[b] Hefei National Laboratory for Physical Sciences at Microscale, University of Science and Technology of China, Hefei 230026, China

ARTICLE INFO

Article history:
Received 1 October 2010
Received in revised form
15 November 2010
Accepted 18 November 2010
Available online 25 November 2010

Keywords:
Methane
CH_4
CH_3D
Titan
Absorption spectroscopy
Cryogenic cell
CRDS
HITRAN

ABSTRACT

The empirical line parameters of over 12,000 methane transitions have been obtained at 80 K in the 1.58 μm transparency window (6165–6750 cm^{-1}) which is of importance for planetary applications. This line list (WKC-80K) was constructed from high sensitivity spectra of normal abundance methane recorded by CW-Cavity Ring Down Spectroscopy at low temperature. The minimum intensity reported is on the order of 5×10^{-30} cm/molecule. High resolution Fourier transform spectra have also been recorded using enriched CH_3D samples at 90–120 K in order to facilitate identification of monodeuterated methane features in the methane line list at 80 K. The CH_3D relative contribution in the considered region is observed to be much larger at 80 K than at room temperature. In particular, CH_3D is found dominant in a narrow spectral window near 6300 cm^{-1} corresponding to the highest transparency region.

Using a similar line list constructed at room temperature (Campargue A, Wang L, Liu AW, Hu SM and Kassi S. Empirical line parameters of methane in the 1.63–1.48 μm transparency window by high sensitivity Cavity Ring Down Spectroscopy. Chem Phys 2010;373:203–10.), the low energy values of the transitions observed both at 80 K and at room temperature were derived from the variation of their line intensities. Empirical lower states and *J*-values have been obtained for 5671 CH_4 and 1572 CH_3D transitions representing the most part of the absorbance in the region. The good quality of these derived energy values is demonstrated by the marked propensity of the corresponding CH_4 lower state *J* values to be close to integers. The WKC line lists at 80 K and room temperature provided as Supplementary Material allow one accounting for the temperature dependence of methane absorption between these two temperatures. The importance of the 80 K line list for the study of Titan and other methane containing planetary atmospheres is underlined and further improvements are proposed. The resulting information will advance the theoretical modeling of the methane spectrum in the 1.58 μm transparency window.

1. Introduction

The present work is devoted to the 1.58 μm transparency window of methane, which is a spectral region of low opacity lying between strong absorption regions corresponding to the polyads of vibrational states called tetradecad and icosad. In a recent contribution [1], we have reported the construction of an empirical list of more than 16,000 transitions for methane at room temperature (RT) in the 6165–6750 cm^{-1} region. The spectra were recorded by high sensitivity Cavity Ring Down Spectroscopy (CRDS) with the help of 27 fibered distributed feedback (DFB)

* Corresponding author.
E-mail address: Alain.Campargue@ujf-grenoble.fr (A. Campargue).

0022-4073/$ - see front matter © 2010 Elsevier Ltd. All rights reserved.
doi:10.1016/j.jqsrt.2010.11.015

lasers [2]. The intensity values span over six orders of magnitude from 1.6×10^{-29} to 2.5×10^{-23} cm/molecule. The achieved sensitivity (noise equivalent absorption $\alpha_{min}\sim3\times10^{-10}\,cm^{-1}$) allowed us to measure line intensities which are three orders of magnitude smaller than the intensity cut off of the HITRAN [3] line list of methane (4×10^{-26} cm/molecule). The number of measured transitions was increased from 2126 in HITRAN to 16223.

Similar performances can be achieved at liquid nitrogen temperature (LNT) by combining a specifically designed cryogenic cell with the CW-CRDS technique [4]. In Ref. [5], we reported the analysis of the central section of the transparency window (6289–6526 cm^{-1}) at LNT and RT because it corresponds to the $3\nu_2$ band of CH_3D which is important for planetary studies. The present contribution completes these initial efforts to construct empirical line lists for the transparency window between 6165 and 6750 cm^{-1}. When a spectral line is observable at both temperatures, the measured line intensities from the RT line list of Ref. [1] and the present LNT line list will be combined to compute effective lower state energy E''. This "two-temperature" method was successfully applied to the tetradecad and icosad regions surrounding the considered transparency window [6–11] and also to the region of the $3\nu_2$ band of CH_3D [5].

Considering the variation of the CH_3D/CH_4 relative abundance in the various sources of methane on Earth [12] and in planetary atmospheres [13], the discrimination of the CH_3D and CH_4 transitions in the spectrum of methane is a prerequisite to satisfactorily account for the transmission in the 1.58 μm window. Apart from the $3\nu_2$ band, many additional CH_3D lines were identified in the RT spectrum [1] through comparison with recent FTS spectra recorded at USTC (Hefei, China) with enriched CH_3D samples. An important result of Ref. [1] was the quantitative evaluation of the CH_3D contribution to the absorption at room temperature. From simulations of the CH_3D and methane spectra at low resolution, the CH_3D isotopologue in "natural abundance" was found to contribute by up to 25% of the absorption in some spectral sections. Due to the high line density of features and their strong temperature dependence, it was sometimes difficult to use the CH_3D spectrum at RT to identify the CH_3D transitions in the LNT spectrum of methane. Therefore, in the present work, new FTS spectra of CH_3D were recorded at low temperature.

After the description of the experimental set up (Section 2) and of the line list construction (Section 3), we will present the procedure followed to identify the CH_3D lines (Section 4). Then the "two-temperature" method will be systematically applied to derive the lower state energy of both CH_4 and CH_3D transitions (Section 5). Finally, possible improvements and applications of the obtained line lists will be discussed in Section 6.

2. Experiment details

The CW-CRDS spectrum of methane at 80 K was recorded at Grenoble University, while FTS spectra of CH_3D at low temperature were recorded at USTC Hefei. Table 1 summarizes the experimental conditions of the recordings.

Table 1
Summary of experimental conditions.

	CW-CRDS of methane	FTS of CH_3D
Gas sample	"natural" gas	CH_3D (> 99%)
Temperature (K)	80 ± 2	90, 120
Sample pressure (Torr)	1.0, 5.0, 10.0	47.5
Path length (m)	NA	0.21
Light Source	DFB laser diode	Tungsten lamp
Beam Splitter	NA	CaF_2
Detector	InGaAs	Ge
Resolution (unapodized) (cm^{-1})	Doppler limited	0.015
Calibration standards	CH_4 [3,14]	H_2O [3]

2.1. CW-CRDS of methane at 80 K

The cryogenic cell specifically designed for CW-CRDS has been described in detail in Refs. [4–6]. The cryostat is a 1.42 m long hollow cylinder both filled and completely surrounded by the sample gas volume. The distance between the high reflective mirrors and the cryostat ends is about 0.5 cm. Instead of the usual piezoelectric actuator that modulates the optical cavity length in standard CW-CRDS, a Mode-by-Mode CRDS acquisition scheme was preferred [4]. The spectra were recorded using the same series of DFB laser diodes used for the RT spectra [1]. A fast (200 Hz) triangular current modulation was applied to the DFB laser while its temperature was slowly ramped from −10 to 60 °C within about 1 h to achieve a spectral coverage of about 35 cm^{-1}. The current modulation leads to a frequency excursion of about 150 MHz, i.e. slightly more than the Free Spectral Range (FSR) of our cavity (106 MHz). The average ring-down repetition rate was close to 500 Hz.

A typical value of $3\times10^{-10}\,cm^{-1}$ was obtained for the noise equivalent absorption [4].

During the recording of both the RT and LNT spectra, the pressure, measured by a capacitance gauge and the ring-down cell temperature were monitored. The LNT spectra were recorded at 1.0, 5.0 and 10.0 Torr. The gas temperature in the cryogenic cell was calculated to be 82 K from the Doppler profile of several tens of lines [4] and 79.6 K from the intensity distribution of the $3\nu_2$ band of CH_3D [5]. The value of 80 ± 2 K is what we refer to as "liquid nitrogen temperature" (LNT).

Each 35 cm^{-1} wide LNT spectrum recorded with one DFB laser was calibrated against the corresponding RT spectrum. The RT spectra were themselves calibrated using the methane positions values provided in the HITRAN database [3] or a high sensitivity FTS spectrum recently recorded in Reims [14] (which was itself calibrated against CO_2 line positions around 6350 cm^{-1}). The precision of the obtained wavenumber calibration estimated from the dispersion of the wavenumber differences is $1\times10^{-3}\,cm^{-1}$.

2.2. FTS of CH_3D at 90 and 120 K

In order to identify the strongest CH_3D lines present in the CRDS spectrum of methane in normal isotopic abundance, spectra of CH_3D at low temperature (90 and 120 K)

were recorded by Fourier Transform Spectroscopy (FTS). The CH_3D sample (stated purity of 99%) was purchased from Sigma-Aldrich. The 21 cm long oxygen-free copper cell was attached to the cold head of a closed-cycle cryostat (Janis SHI-4-5). Two BaF_2 windows were adapted to seal the cell with indium wire. A LakeShore 331S controller was used to control the heating current in a wire attached to the cold head. In this way, the temperature can be adjusted in the range 70–300 K with a 0.2 K accuracy. The temperatures in the middle and end of the cell were monitored by two platinum resistance sensors. The measured temperature difference was less than 1.5 K. The high-resolution spectra of CH_3D were recorded with a Bruker IFS 120HR Fourier transform spectrometer. The entire optical path was evacuated to avoid the atmospheric absorption. A tungsten source, a Ge detector, and a CaF_2 beam-splitter were used. The unapodized spectral resolution was 0.015 cm^{-1}. The line positions were calibrated using H_2O lines listed in the HITRAN database [3].

3. Construction of the line list at 80 K

The same procedure as described in Ref. [5] was followed to construct the line list. The line intensity, S_{v_0}(cm/molecule), of a rovibrational transition centered at v_0, was obtained from the integrated absorption coefficient, A_{v_0} (cm^{-2}/molecule)

$$A_{v_0}(T) = \int_{line} \alpha_v dv = S_{v_0}(T)N \quad (1)$$

where v is the wavenumber in cm^{-1}, $\alpha(v)$ the is absorption coefficient in cm^{-1} obtained from the cavity ring down time, and N the is molecular concentration in molecule/cm^3 obtained from the measured pressure value: $P=NkT$.

The mode by mode scheme adopted for the acquisition of the CRDS spectra at LNT [4], leads to a reduced number of data points defining each line profile: the full profile is described by about six points separated by the FSR of the cavity (106 MHz). This reduced number of data points does not prevent a satisfactory fitting of the profile as it is compensated by the extreme precision on the corresponding frequencies separated by exactly the FSR.

An interactive multi-line fitting program was used to reproduce the spectrum [15]. A Voigt function of the wavenumber was adopted for the line profile as the pressure self broadening has a significant contribution: at 80 K and 10 Torr, the self broadening (HWHM 2.6×10^{-3} cm^{-1} [16]) is about half the Doppler broadening (HWHM 5.0×10^{-3} cm^{-1}). The HWHM of the Gaussian component was fixed to its theoretical value for $^{12}CH_4$. In the case of blended lines or lines with low signal to noise ratios, the Lorentzian HWHM

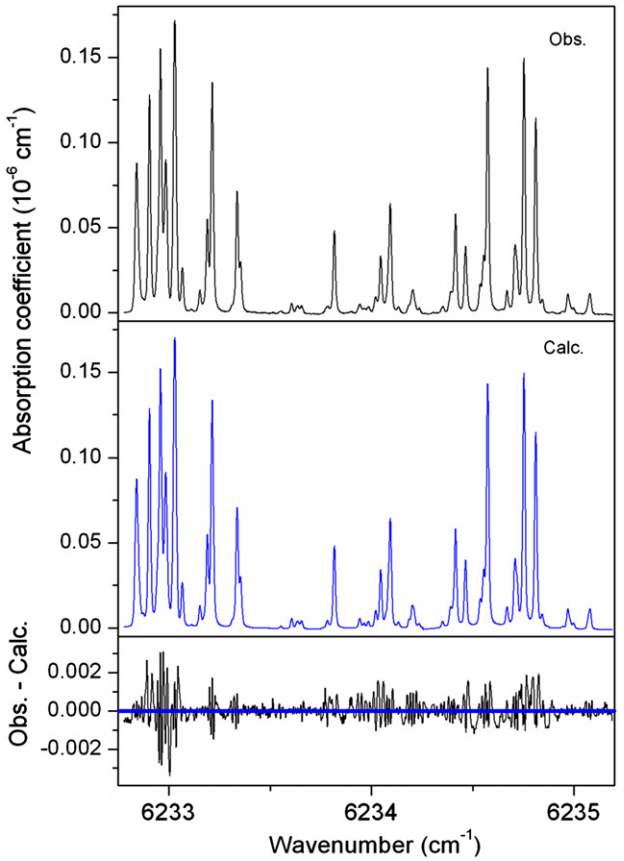

Fig. 1. An example of simulation of the CH_4 spectrum recorded at LNT near 6234 cm^{-1}. From top to bottom: *Upper panel:* experimental spectrum at LNT (P=10.0 Torr), *Middle panel:* Simulated spectrum resulting from the line fitting procedure (a Voigt profile was affected to each line), *Lower panel:* residuals between the simulated and experimental spectra.

was also constrained to the average value obtained from nearby lines.

The average density of lines is more than 20 lines cm^{-1}. This high density and frequent overlapping of the lines made the fitting of the spectrum a very laborious task. Fig. 1 shows an example of comparison between the measured and fitted spectra. Some differences between the observed and simulated spectra are noted. They are partly due to the small sections of warm gas lying between the ends of the cryostat and the supermirrors (see below).

The complete line list at LNT was obtained by gathering the line lists corresponding to the different DFB laser diodes. The final LNT dataset consists of 12268 lines with intensity values ranging from about 6×10^{-30} to 7×10^{-24} cm/molecule for methane in natural abundance at 80 K. The overview of the RT [1] and LNT line lists is presented in Fig. 2. The minimum value of the line intensities detected at LNT is about a factor 10 lower than at RT. This is the result of the increase by a factor of 2 of the peak depths due to the narrowing of the Doppler profile at 80 K, and to the increase by a factor of 4 of the molecular density at 80 K (at a given pressure value).

The change induced by cooling from RT and LNT is considerable both at high resolution (see for instance Figures 2, 3 and 6 of Ref. [5]) and low resolution. We present in Fig. 3 an overview comparison of the low resolution spectrum absorption spectrum of methane (P=1.0 Torr) simulated from the line lists at 296 and 80 K. The spectra were obtained by affecting a normalized Gaussian profile (FWHM = 10.0 cm^{-1}) to each line. It is important to note that the region of highest transparency is significantly shifted to lower energy at 80 K. This is mainly due to a sharp decrease in the high-J line intensities of the tetradecad R-branch transitions between 6200 and 6300 cm^{-1}.

4. Identification of the CH_3D transitions

The quantitative evaluation of the CH_3D contribution to the absorbance in the considered region is important because the CH_3D/CH_4 relative abundance (and then the opacity) varies significantly depending on the considered planetary atmospheres [13]. Due to the large difference of the CH and CD stretching frequencies, the second overtone of the CD stretch of CH_3D, $3\nu_2$, falls in the center of the transparency window. This band was used to determine the D/H ratio in Uranus [17], Neptune [13] and Titan [18,19]. In its most recent version, the HITRAN line list for methane includes the line parameters of the $3\nu_2$ band as obtained 25 years ago from FTS spectra recorded with a highly enriched CH_3D sample [20–22]. Taking into account the relative abundance factor adopted in HITRAN (6.15×10^{-4}) [3], the $3\nu_2$ band of CH_3D has line intensities ranging between 4.3×10^{-27} and 2.5×10^{-26} cm/molecule. These values are below the 4×10^{-26} cm/molecule intensity cut off adopted in the HITRAN database for the main isotopologue but well above of our sensitivity

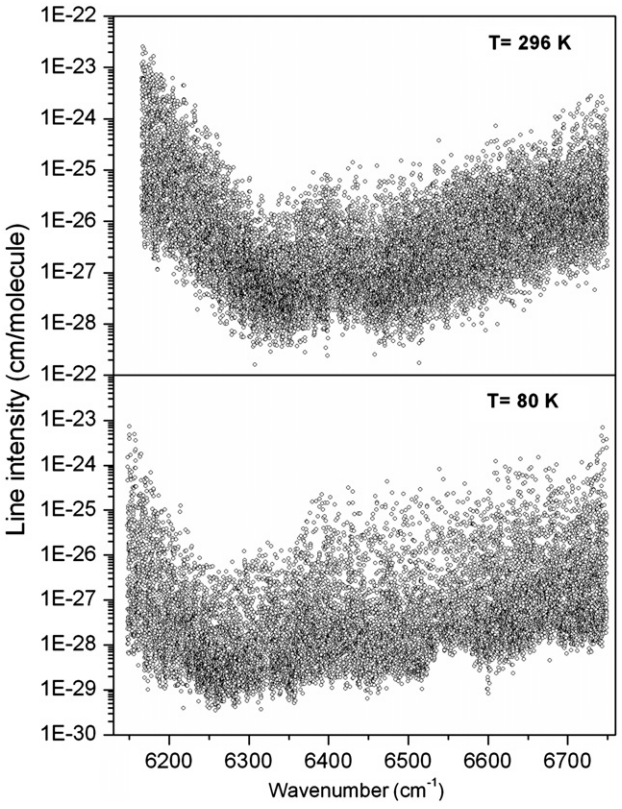

Fig. 2. Overview comparison of the line lists constructed from the CRDS spectrum of methane at 296 K (upper panel) and 80 K (lower panel) in the 6150–6750 cm^{-1} region.

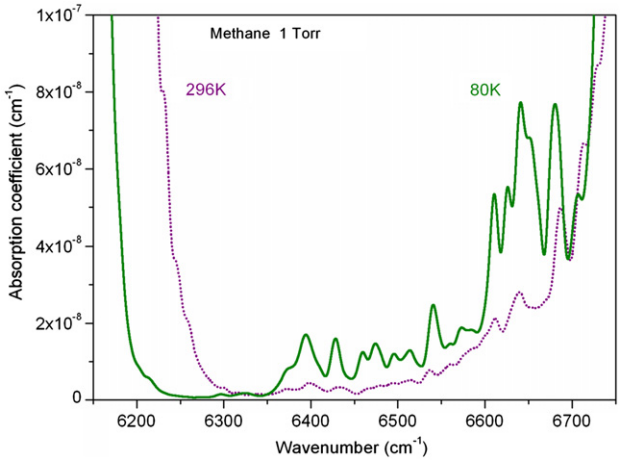

Fig. 3. Comparison of the 'low resolution' absorption spectrum of methane (P=1.0 Torr) simulated from the CW-CRDS line lists at 296 K (short dot) and 80 K (full). The spectra were obtained by affecting a normalized Gaussian profile (FWHM=10.0 cm^{-1}) to each line.

threshold. Practically all the $3\nu_2$ transitions of CH_3D listed in the HITRAN database [3,20] were identified in our RT and LNT spectra of methane in "natural" abundance [1,5]. An important result of Ref. [1] is the evidence of a systematic 18% deviation of the CH_3D intensities in our methane spectra compared with HITRAN values. This apparent discrepancy was explained [1] by the difference between the CH_3D/CH_4 abundance ratio in our sample (about 5×10^{-4}) and the relative abundance adopted in HITRAN (6.15×10^{-4}). The evidenced 18% difference coincides with the usual value of CH_3D depletion in "natural gas" on Earth [12] and leads to a CH_3D abundance in our sample ($\sim5\times10^{-4}$) very close to the value in the Titan atmosphere [23–25].

4.1. RT spectrum

As mentioned in the Introduction, the CH_3D lines present in the RT line list were previously identified in Refs. [1,5] by comparison with our FTS spectra of CH_3D. Apart from the $3\nu_2$ transitions of CH_3D listed in the HITRAN database, a high number of additional CH_3D lines were found. They are marked by "D" in the RT line list attached as Supplementary Material of Refs. [1,5]. Also some lines (marked with H/D) were found to have a significant contribution of both CH_3D and CH_4. All the other lines were believed to be due to $^{12}CH_4$ (or $^{13}CH_4$) and are marked with "H" in the RT list [1,5].

4.2. LNT spectrum

The identification of the CH_3D transitions in the LNT spectrum is more difficult. Apart from the $3\nu_2$ transitions which are rotationally assigned, the temperature dependence of the methane line intensities is unknown. In Ref. [5] dedicated to the $3\nu_2$ region, we decided to transfer the species determination from the RT line list to the LNT line list: if the difference, δ, of the centers of lines observed in the RT and LNT CRDS spectra differed by less than 0.002 cm^{-1}, the two lines were believed to correspond to the same transition and then to the same species. Although the chosen 0.002 cm^{-1} value is very strict (it corresponds to one fifth of the FWHM Doppler width at 80 K), this method using the line center values as the only criterion may lead to some errors in the (few) cases when a CH_4 line observed at RT has a much weaker intensity at LNT and is blended with a CH_3D line which dominates at LNT. Another drawback is that nearly 60% of the lines (all weak or very weak) observed at LNT but unobserved at RT were deprived of isotopologue determination. This is in particular the case in the region near 6300 cm^{-1} where CH_3D transitions are completely obscured in the RT spectrum by strong CH_4 transitions which vanish at LNT revealing a high number of CH_3D lines.

This is why in the present work, low temperature FTS spectra of CH_3D were recorded at USTC Hefei to identify CH_3D lines using both the positions and intensities coincidences. Fig. 4 shows an overview comparison of the CH_3D FTS spectra at 120 K and RT. In spite of a short absorption path length, many CH_3D transitions were detected in addition to the $3\nu_2$ transitions. The $3\nu_2$ band is accompanied by a number of lines around 6300 cm^{-1} which are particularly important as they contribute to the absorption in the spectral section of highest transparency. Fig. 5 shows a spectral section near 6296 cm^{-1} where most of the lines observed at 80 K are unambiguously attributed to CH_3D while they are obscured by much stronger CH_4 lines in the RT spectrum.

Fig. 5 shows that, in spite of the small relative abundance of CH_3D in the CRDS spectrum ($\sim5\times10^{-4}$), the sensitivity of our FTS spectrum of a highly enriched CH_3D sample is not sufficient to allow for the identification of the very weak CH_3D lines. Considering the noise level of the FTS spectrum, we estimate the intensity threshold of the CH_3D lines in the LNT CRDS spectrum to be 2×10^{-27} cm/molecule, which could be surely attributed to CH_3D. Below this value, the identification of the CH_3D transitions at LNT was based on the position coincidence ($\delta<$ 0.003 cm^{-1}) with the FTS spectrum of CH_3D at room temperature. As a consequence, the CH_3D label (D) of the lines with intensities lower than 2×10^{-27} cm/molecule is less

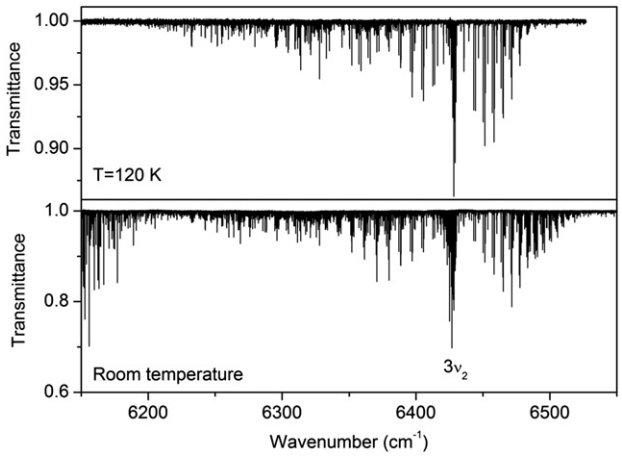

Fig. 4. Overview comparison of the FTS spectra of CH_3D (99% stated purity) recorded at 120 K and room temperature in the 6150–6550 cm^{-1} region. The sample pressure and the absorption pathlength were 4.17 Torr of 15 m at room temperature and 47.5 Torr and 21 cm at 120 K. Note the clear reduction of the extension of the P- and R-branches of the $3\nu_2$ band at 6425 cm^{-1} and that many lines not belonging to $3\nu_2$ are detected in the 6250–6350 cm^{-1} section.

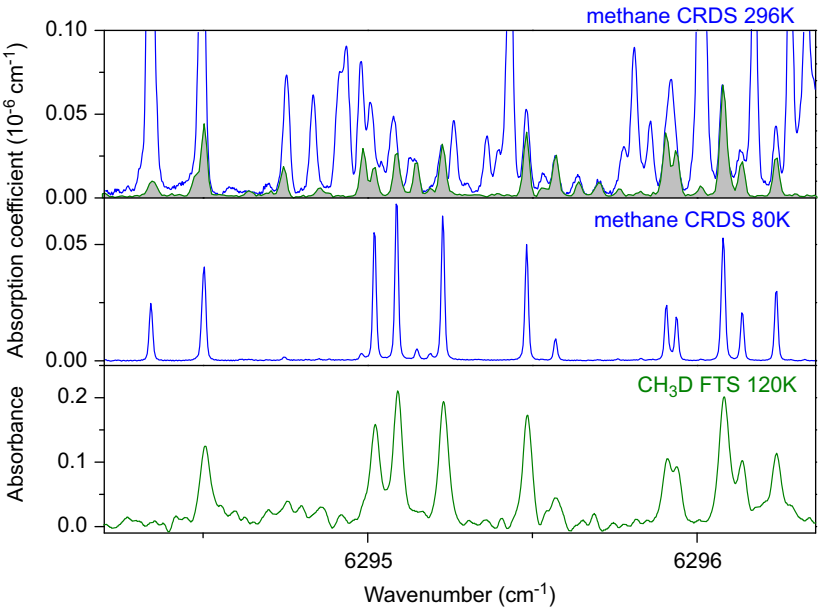

Fig. 5. Identification of the CH_3D transitions in the CRDS spectrum of methane at 80 K (middle panel) by comparison to the FTS spectrum of CH_3D recorded at 120 K (lower panel). The room temperature CRDS spectrum of methane is displayed on the upper panel with the corresponding room temperature FTS spectrum of CH_3D. In the displayed region, the CH_3D transitions dominate the 80 K spectrum of methane while they are totally obscured by the much stronger CH_4 lines at room temperature (upper panel). The line near 6294.34 cm^{-1} observed in the CRDS spectrum (middle panel) and missing in the FTS spectrum of CH_3D is a CH_4 line.

reliable than that for the stronger lines. Finally, we affected a D* label indicating a less secure CH_3D identification for the very few transitions which are not observed in the CH_3D FTS spectrum at room temperature and correspond to lines near the noise level in the CH_3D cold FTS spectrum. Note that in both lists attached as Supplementary Material, the CH_3D transitions of the $3\nu_2$ band are indicated by a label ($3\nu_2$).

In summary, for both RT and LNT CRDS spectra of methane, we have used a FTS spectrum of CH_3D recorded in similar temperature conditions to find all the CH_3D lines at RT and the CH_3D lines stronger than 2×10^{-27} cm/molecule at low temperature.

All the lines with intensities larger than 2×10^{-27} cm/molecule which are not CH_3D lines were marked as CH_4 lines. In addition, we transferred the CH_4 identification from the RT line list: if a line has a center at LNT which coincides within 0.003 cm^{-1} to a CH_4 line at RT, it was marked as CH_4.

At the end of the procedure, among the 12268 lines measured at LNT, 5671 were assigned to CH_4 (either $^{12}CH_4$

or $^{13}CH_4$) and are marked with (H), 1572 were assigned to CH_3D (D, D*) and 450 were found to have a significant contribution of both isotopologues (H/D). The large set of 4575 very weak lines left without species identification represents less than 1% of the total absorbance in the region and must be attributed in its large majority to CH_4. Table 2 presents the summary of the species identification at RT and LNT both in terms of the number of lines and the corresponding intensities. Note that the total absorbance in the region decreases by almost a factor of 10 by cooling from RT to LNT because of the sharp decrease of the intensities of the high-J lines of the R-branches of the high-energy bands of the tetradecad below 6250 cm^{-1}.

Fig. 6 shows an overview of the RT and LNT line lists where the CH_3D transitions (those marked with D and D* in the line lists) have been highlighted.

In order to further quantify the CH_3D contribution to the methane absorption in the region, we have included in Fig. 6 (right hand side) a low resolution simulation calculated from the CRDS line lists at RT and LNT. The spectra were obtained by affecting a normalized Gaussian profile (FWHM = 10.0 cm^{-1}) to each line. The CH_3D contribution is indicated at both temperatures. Interestingly, the obtained absorbances show that the CH_3D relative contribution is much more important at LNT than at RT: while it represents at maximum about 25% of the total absorption near the Q-branch of the $3\nu_2$ band at 6430 cm^{-1} and in the lowest opacity region near 6320 cm^{-1}, CH_3D is by far the main absorber in the 6250–6350 cm^{-1} micro-window of the LNT spectrum. This is mainly due to the decreased intensity of high-J lines arising from the R branches of the tetradecad below 6300 cm^{-1} and from the P-branch lines of the icosad ($5\nu_4$) above 6600 cm^{-1}, leading a 100 cm^{-1} spectral interval where the remaining absorption is essentially due to CH_3D.

We have superimposed to the low resolution spectra at RT (Fig. 6 upper panel, right hand side), a low resolution

Table 2
Summary of the observations and corresponding intensities of the CH_3D and CH_4 transitions measured by CRDS at 296 and 80 K between 6165 and 6750 cm^{-1}.

	CH_4 (H)[a]	CH_3D (D,D*)[a]	Blended (H/D)[a]	Total
		Number of lines		
296 K	13714	1393	1116	16223
80 K	5671+4575 (no mark)	1572	450	12268
		Intensity (cm/molecule)		
296 K	1.29×10^{-21} (99.81%)	1.56×10^{-24} (0.12%)	8.96×10^{-25} (0.069%)	1.30×10^{-21}
80 K	1.45×10^{-22} (97.3%)+1.07×10^{-24} (0.72%) (no mark)	2.62×10^{-24} (1.76%)	2.33×10^{-25} (0.16%)	1.49×10^{-22}

[a] See text (Section 4) for the definition of the different labels (H, D, D*, H/D)

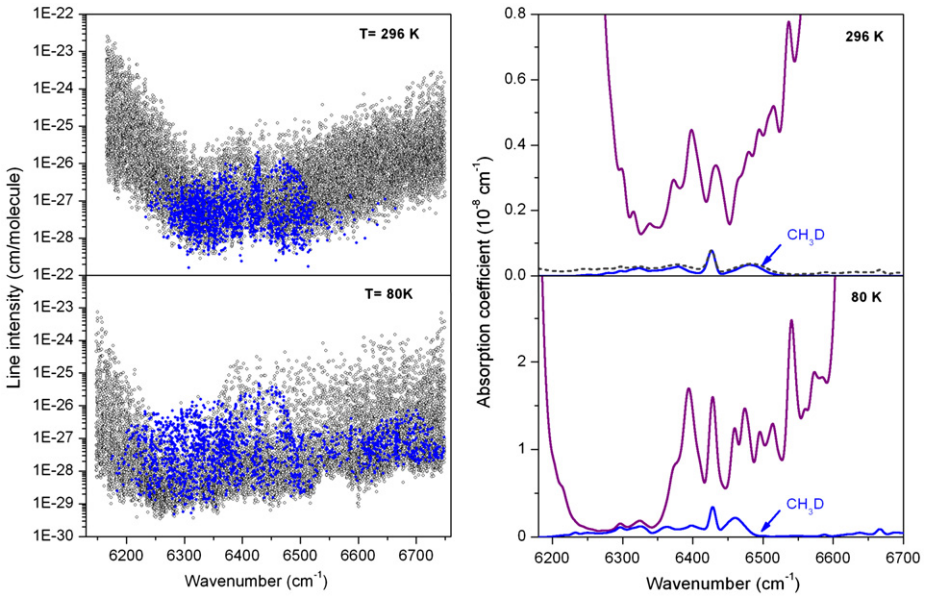

Fig. 6. Contribution of the CH_3D transitions to the methane absorption between 6150 and 6750 cm^{-1} at room temperature (upper panels) and 80 K (lower panels) *Left hand*: the CH_3D transitions have been highlighted in blue. *Right hand*: corresponding low resolution simulations (P = 1.0 Torr) obtained from the complete line list (purple) and limited to the CH_3D lines (blue). Note that while CH_3D transitions represent at most 25% of the absorption at room temperature, it represents most of the absorption at 80 K near 6300 cm^{-1}. On the upper panel, the low resolution FTS spectrum of CH_3D has been superimposed to the CW-CRDS spectrum of methane. (For interpretation of the references to colour in this figure legend, the reader is referred to the web version of this article.)

simulation of the FTS spectrum of CH_3D at RT with intensities scaled in order to match the intensities of the $3\nu_2$ band in our CRDS spectrum [5]. The obtained low resolution spectrum shows that the proportion of "missing" CH_3D lines in the RT list is important only in the region where the CH_3D lines could not be identified as they are obscured by much stronger CH_4 lines.

In a very recent contribution, Ulenikov et al. [26] reported a global rovibrational analysis of the infrared FTS spectrum of CH_3D at 80 K. We have performed a systematic comparison of the line list attached to Ref. [26] with the CH_3D transitions in our methane line list at 80 K. As no intensity information is provided in Ref. [26], the comparison was performed only for the line positions and the lower state energies. In our region of interest, Ulenikov et al. assigned 240 rovibrational transitions to the $\nu_1+\nu_2+\nu_6$ E, $\nu_2+\nu_4+\nu_6$ A_1 and $3\nu_2$ A_1 bands at 6298.488, 6337.064 and 6428.364 cm^{-1}, respectively. As illustrated in Fig. 7, they represent only a small fraction of the 1572 CH_3D transitions in our line list of methane in "natural" abundance at 80 K. 206 of the 240 transitions of Ref. [26] are included in our line list, the others being hidden by much stronger CH_4 transitions. The comparison of the line positions leads to an average $(\nu_{CRDS}-\nu_{Ulenikov})=-1.2\ (6)\times 10^{-3}\ cm^{-1}$. For about half of the transitions in common, we could derive the empirical values of the lower state energy by using the two-temperature method (see next Section). The comparison of our empirical values to the low energy values calculated from the assignments of Ref. [26] leads to an average relative deviation $(E_{emp}-E_{Ulenikov})/E_{Ulenikov}=-3.4\ (13.4)\%$. This result is very satisfactory considering that our empirical lower energy values rely on intensity measurements of CH_3D in methane in normal abundance.

In the absence of a high-sensitivity spectrum of the $^{13}CH_4$ isotopologue, the $^{12}CH_4$ and $^{13}CH_4$ transitions could not be discriminated. The $5\nu_4$ bands of $^{13}CH_4$ are predicted to be affected by an isotopic shift of some tens of wavenumbers compared with the $5\nu_4$ bands of $^{12}CH_4$ [27]. The $^{13}CH_4$ bands being shifted to lower energy, i.e. to the region of weaker absorption; the $^{13}CH_4$ relative contribution to the absorbance in the 6350 cm^{-1} region is expected to be larger than the 1.1% relative abundance of this isotopologue. Nevertheless, this effect is expected to be limited and not comparable with the CH_3D situation.

5. Determination of the lower energy values of the transitions

Following earlier works by Margolis [28] and Pierre et al. [29], in the high-absorbing regions surrounding the presently studied transparency window, we have systematically used the ratio of the line intensities measured at LNT and RT to determine the low-energy levels of the transitions in common in the two spectra [5–11]. As a consequence of the large difference between the two temperatures of our recordings, the "two-temperature" method was found to be a particularly efficient and robust method to account for the temperature dependence of the methane absorption.

The lower-state energy, E, of a given transition is related to the ratio of line intensities at two temperatures [6]:

$$\ln\left(\frac{S_{\nu_0}(T_1)Z(T_1)}{S_{\nu_0}(T_0)Z(T_0)}\right)=-E\left[\frac{1}{kT_0}-\frac{1}{kT_1}\right] \quad (2)$$

where T_0 and T_1 are the RT and LNT, respectively and S_{ν_0} are the corresponding line intensities.

From the values of the partition function at 296 and 80 K given in HITRAN for $^{12}CH_4$ [3], we obtain $Z(296\,K)/Z(80\,K)=7.05337$. This value differs by less than 1% from the value (7.117) adopted in our previous works assuming a $T^{3/2}$ temperature dependence of the rotational partition function [5–11]. Note that the $Z(296\,K)/Z(80\,K)$value obtained for $^{12}CH_4$ is very close to the corresponding values for $^{13}CH_4$ (7.05346) and CH_3D (7.07757) and the two-temperature method can be applied independently of the methane isotopologue.

The automatic association of the lines in the RT and LNT datasets relies on the coincidence of their centers (obviously they should also be assigned to the same isotopologue in the

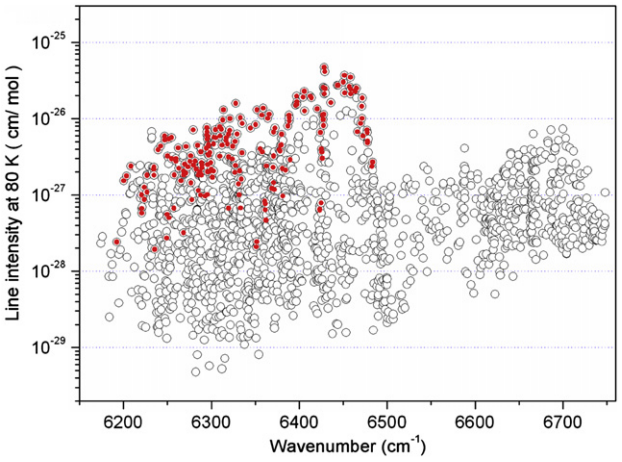

Fig. 7. Overview comparison of the transitions attributed to CH_3D in the list of methane at 80 K (1572 lines) with the CH_3D transitions rovibrationally assigned in Ref. [26] (240 lines). The 206 lines in common are highlighted. No intensity information is provided in Ref. [26].

two datasets). As in our preceding contributions [5–11], a strict criterion is chosen to insure that a RT line and a LNT line correspond to the same transition: the difference, δ, of their centers must differ by less than 0.002 cm^{-1}. This value takes into account the average uncertainties on the two line center determinations and corresponds to one fifth and one tenth of the Doppler width (FWHM) at LNT and RT, respectively. According to this criterion, 4503 and 591 pairs of transitions were found in coincidence for CH_4 and CH_3D, respectively. They are highlighted in the overview plots presented in Fig. 8. Overall, the associated transitions represent 81.5% and 87.9% of the total absorbance at RT and LNT, respectively.

Using Eq. (1) above, the lower-energy values, E, were empirically determined. In the case of both $^{12}CH_4$ and $^{13}CH_4$, the rotational energy levels are well separated and the corresponding empirical J-values can be computed from $J_{emp}=\sqrt{(1/4)+(E/B_0)}-(1/2)$, where B_0=5.214 cm^{-1} is the $^{12}CH_4$ (and $^{13}CH_4$) ground-state rotational constant. The above expression based on a simple rigid rotor approximation is sufficient as the splitting of the tetrahedral multiplets remains small in our range of J-values (for instance 0.5 cm^{-1} at J=12) [30]. Since CH_3D is a symmetric top molecule, the values of the rotational levels are too dense to unambiguously derive empirical values of the J and K quantum numbers from the empirical E-value. As an example, the CH_3D transitions and the obtained empirical J-values of the CH_4 transitions are indicated on the RT and LNT spectra displayed in Fig. 9.

In Fig. 10, the empirical J-values are plotted versus the CH_4 line centers. The observed propensity of the empirical J-values to be close to integers is a good indication of the quality of the obtained results. In Fig. 11, the corresponding histograms are presented both in terms of numbers of lines and of the corresponding sum of their intensities. As usual [5,7–10], the contrast between integer and non-integer J-values is more pronounced for the intensities than for the number of lines. This is due to the fact that the uncertainty on the line intensity values (and then on the J-values) is larger for the weaker lines and then, on average, non-integer J-values correspond to smaller intensities. 70% of the J determinations lead to J-values falling within a ± 0.25 interval around integer values. These "integer" J-values correspond to 88% of the total absorbance at 80 K.

Our previous studies [5,7–10] showed that the $\delta < 0.002$ cm^{-1} criterion is too strict in the case of strongly blended or very weak lines and that additional pairs of lines correspond undoubtedly to the same transitions and should be associated. We decided to relax the coincidence criterion on the line centers and increased it up to 0.003 cm^{-1} which allowed us to derive 812 additional low-energy determinations representing 4.7% of the total absorbance at both LNT and RT. As the derived low-energy values of the lines with $0.002 < \delta < 0.003$ cm^{-1} are expected to be less accurate, they are marked (*) in the line lists provided as Supplementary Material.

The complete sets of transitions measured at 80 and 296 K are provided as two separate Wang-Kassi-Campargue (WKC) line lists: WKC-80K.txt and WKC-296K.txt. They include the species identification, the lower-state energy values for the pairs of associated transitions, together with the empirical J-values for the CH_4 isotopologues. Table 3 gives a sample of the LNT line list.

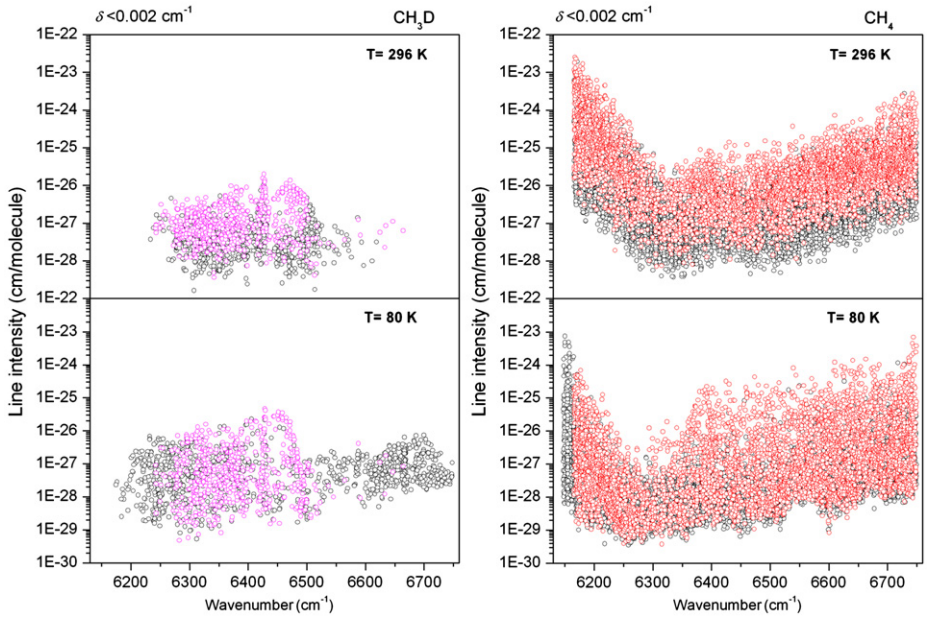

Fig. 8. Overview of the spectrum of CH_3D (left hand) and CH_4 (right hand) between 6150 and 6750 cm^{-1} as obtained from the analysis of the CW-CRDS spectra at 296 K (upper panel) and 80 K (lower panel). The transitions for which the lower energy value was derived from the ratio of the line intensities ($\delta < 0.002$ cm^{-1}) are highlighted with pink and red symbols for CH_3D and CH_4, respectively. (For interpretation of the references to colour in this figure legend, the reader is referred to the web version of this article.)

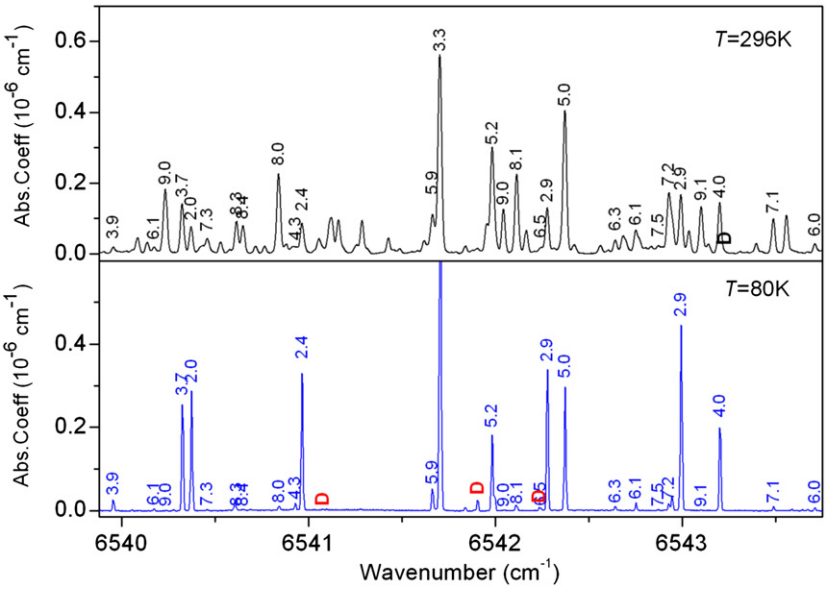

Fig. 9. Comparison of the CW-CRDS spectra of methane at liquid nitrogen temperature (lower panel) and room temperature (upper panel) near 6542 cm^{-1}. The RT and LNT spectra were recorded with pressures of 10.0 and 1.0 Torr, respectively. The few CH_3D transitions observed in the region are marked with "D". The empirical *J*-values obtained from the temperature variation of the line intensities are indicated for the CH_4 isotopologue.

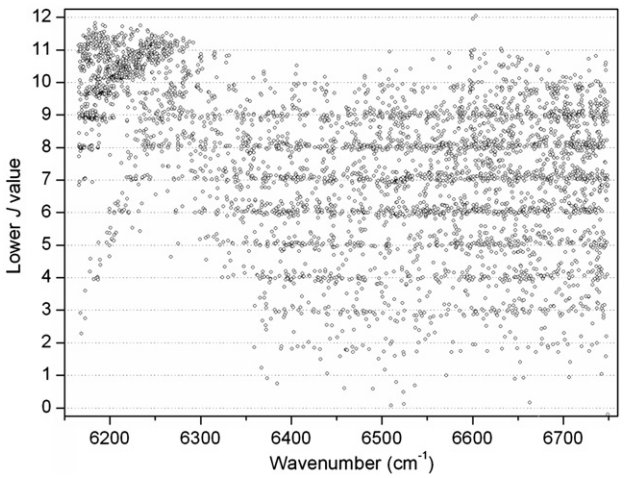

Fig. 10. Empirical *J*-values of the CH_4 transitions observed between 6150 and 6750 cm^{-1} versus the transition wavenumbers.

5.1. Distortion of the high empirical J-values

The histograms relative to the number of CH_4 lines and to their intensities at RT (Fig. 10 upper and middle panel, respectively) show that the integer–non integer alternation disappears above $J=10$ and that the obtained empirical *J*-value distribution sharply decreases above this value. Such behavior was already noted in our previous studies but is much more pronounced in the presently investigated region as high-*J* transitions of the strong bands of the tetradecad are sufficiently strong to be detected at 80 K below 6300 cm^{-1}. A possible explanation of the appearance of the histograms for high-*J* values is the weakness of the corresponding transitions in the low-temperature spectrum which may lead to larger uncertainties in the retrieved intensity values and then on the J_{emp} values. For instance, the intensity of a $J=11$ transition is divided by about a factor 1075 by cooling from 296 to 80 K. Nevertheless, larger uncertainties in the intensities would lead to a random dispersion of the empirical *J*-values around integer values while a careful examination of Fig. 10 shows that around $J=10$, the empirical *J*-values appear systematically shifted down to about 9.6.

Such a systematic effect is in fact due to the small sections of warm gas lying between the ends of the cold jacket and the windows of the cryogenic cell [4]. The external stainless steel cylinder is 1.4 m long ($\Phi=6.3$ cm diameter) while the cryostat is made of two co-axial tubes ($\Phi=1.6$ and 2 cm) joined at the ends by two rings. The distance between the cryostat ends and the high-reflective

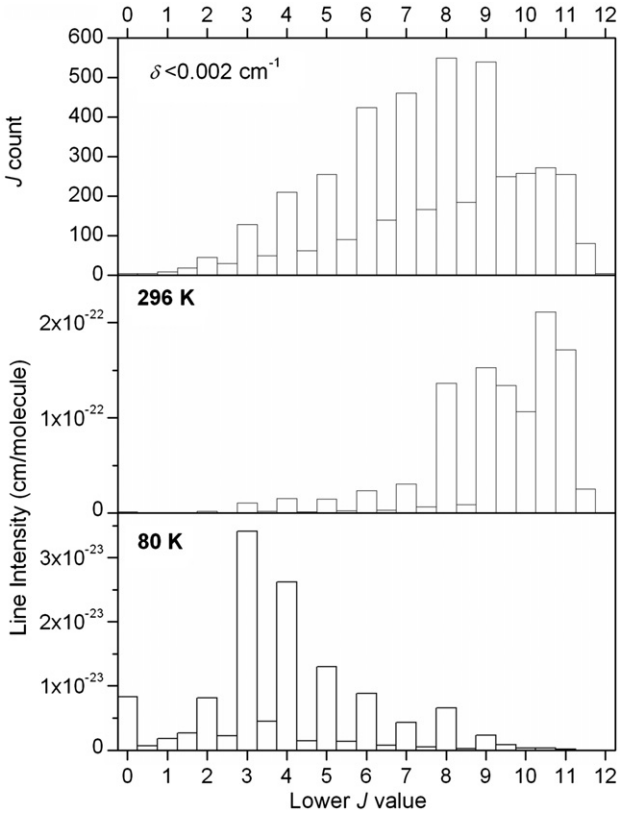

Fig. 11. Histograms of the empirical J-values determined for the CH_4 transitions (step interval of 0.5). The upper panel is relative to the number of lines. In the two lower panels, the corresponding RT and LNT line intensities were added for each step interval. Note that the contrast between integers and non integers is more pronounced in terms of intensities than in terms of number of lines (see Text).

mirrors is only 6 mm (at RT). Inside the inner tube, the gas sample rapidly equilibrates to the cryostat temperature but in the intermediate space between the cryostat and the mirrors, the gas temperature is expected to increase from 80 K to a value approaching room temperature. Compared with a cryogenic cell with a uniform low temperature, this warmer section of gas leads to an overestimation of the LNT intensities of the high-J transitions and then an underestimated empirical value of J. Taking into account the 4 mm contraction of the cryostat at LNT, the total path-length ouside the cryostat is 16 mm, i.e. only 1.1% of the total path length. This temperature gradient has a negligible effect for J-values lower than 9 but for higher J-values, the situation is different due to the steep decrease in the LNT line intensities. For instance, a J=11 line has its intensity divided by more than 3 orders of magnitude at 80 K and the 1% section of warm gas is expected to have a larger contribution to the measured intensity than the 99% section of the cell at 80 K.

In order to quantify this effect, we have considered a simple model assuming a linear dependance of the gas temperature between 80 K at the ends of the cryostat and 290 K on the mirrors (the measured temperature of the outside cylinder is about 290 K). Fig. 12 shows the ratio, r, of the line intensities for a cell with such a temperature gradient and a cell at a uniform temperature of 80 K. The obtained curve (plotted in logarithmic scale) shows that while the warm gas has practically no impact below J=9, it begins to dominate the absorption at J=10. Using the correction factor, r, on the line intensities, the deviation of the retrieved J-value from their real value can be computed. It leads to the curve included in Fig. 12 which gives for J=10 an apparent J-value very close to the value of 9.6 estimated from Fig. 12. The apparent J-values increase very slowly above J=10 with an asymptote around J_{emp}=11 in good agreement with the histograms of Fig. 11.

It is worth emphasizing that high-J lines with distorted lower-J values and therefore inaccurate temperature dependence are completely negligible at low temperature and have a significant contribution at room temperature only in the small 6200–6250 cm^{-1} interval where the high-J lines of the R branches of the tetradecad are located (see Fig. 10). The experimental evidence of the distortion of the very weak intensities of the high-J lines illustrates the high dynamics in the intensity values (more than 4 decades) which can be measured with our CW-CRDS spectrometer.

6. Discussion

6.1. Comparison with the GOSAT line list

In relation with the "Greenhouse Gases Observing Satellite" (GOSAT) project [31], a line list has recently

Table 3
Wavenumbers and line strengths of the methane transitions measured at 80 K by CW-Cavity Ring Down Spectroscopy near 6591 cm^{-1}. This table is a small section of the WKC-80K list of 12268 transitions between 6165 and 6750 cm^{-1} which is provided as Supplementary Material.

ISO[a]	T=80 K		T=296 K [1]			
	Center (cm^{-1})	Intensity (cm/mol)	Center (cm^{-1})	Intensity (cm/mol)	E (cm^{-1})	J_{emp}
H	6591.1405	1.428E−26	6591.1406	4.289E−27	56.809	2.83
H	6591.1761	7.464E−26	6591.1762	4.283E−26	105.798	4.02
D	6591.2185	9.197E−29	6591.2170	4.790E−28	272.712	
	6591.2554	1.285E−28				
H	6591.2694	7.961E−28	6591.2684	3.157E−27	252.084	6.45
H	6591.2921	1.597E−26	6591.2924	5.138E−26	236.259	6.23
H	6591.3241	1.706E−27	6591.3251	3.185E−26	369.322	7.91
H	6591.4603	2.540E−27				
H	6591.4943	5.741E−27	6591.4954	1.650E−26	227.722	6.11
H	6591.5528	4.794E−27	6591.5518	1.521E−26	235.204	6.22
H	6591.6129	3.305E−28	6591.6129	7.561E−27	384.704	8.08
	6591.6195	1.438E−28				
H	6591.6530	4.021E−27	6591.6526	2.774E−26	293.984	7.01
H	6591.6861	2.819E−26	6591.6862	8.571E−26	231.981	6.17
H	6591.7354	4.068E−29	6591.7376	1.976E−27	441.682*	8.69*
	6591.7641	5.600E−29				
H	6591.7752	1.235E−28	6591.7770	2.100E−27	362.251	7.83
	6591.7873	1.926E−28				
	6591.7958	2.026E−28				
	6591.8038	2.137E−28				
H	6591.8234	1.676E−27	6591.8248	2.255E−26	344.534	7.62
H	6591.8992	5.520E−27	6591.9004	2.445E−27	86.206	3.59
H	6591.9978	2.740E−28	6591.9983	7.041E−27	393.499	8.18
H	6592.0573	1.976E−28	6592.0567	4.640E−27	386.677	8.10
H	6592.0687	5.174E−28	6592.0682	4.161E−26	479.836	9.08

Notes: Low energy values, E, were obtained for the transitions whose center coincides with that of a line observed in the 296 K spectrum ($\delta < 0.002$ cm^{-1}). The "*" symbol in the last column marks the lines whose RT and LNT line centers differ by $0.002 < \delta < 0.003$ cm^{-1}. For CH_4, the empirical J-values are given in the last column.

[a] Isotopologue: "H" corresponds to both the $^{12}CH_4$ and $^{13}CH_4$ isotopologues while "D" corresponds to CH_3D (see text).

become available for methane at room temperature in the 550–6236 cm^{-1} range [32]. This line list was constructed from FTS spectra recorded with a coolable White-type cell in a large variety of temperature and pressure conditions. The intensity cut off of the GOSAT line list (about 4×10^{-26} cm/molecule) is two orders of magnitude lower than that of the Margolis line list [33] included in the HITRAN database in that region and equivalent to that of Brown's list [34] adopted for HITRAN above 6180 cm^{-1}. The GOSAT line list which covers the whole tetradecad from 5550 to 6236 cm^{-1} can be compared with our present results in the 6165–6236 cm^{-1} overlapping region. Fig. 13 shows the important gain in terms of sensitivity: the CRDS line list at RT includes1876 transitions while the GOSAT line list is limited to the 437 strongest lines. The additional lines detected by CRDS add 12.7% to the total GOSAT absorbance in the region. We have also included in this figure the overview comparison of the CRDS line list at LNT to the line list previously constructed from spectra recorded by Differential Absorption Spectroscopy (DAS) at LNT [10]. While the intensity cut off of the GOSAT and DAS is similar, the gain in sensitivity is even more pronounced compared with DAS at LNT.

6.2. Possible improvements of the line lists

In principle, theoretical analysis may provide valuable information to improve our empirical line list. For instance, the empirical values of the lower-state energy may be replaced by their exact values when the transitions have been fully assigned on a theoretical basis. Unfortunately, theoretical analyses are very scarce and still in progress in our region. A partial modeling of the tetradecad region on the basis of the GOSAT line list was recently reported [32]. In the 6165–6236 cm^{-1} region overlapping with GOSAT dataset, 73 of the 437 transitions were fully rovibrationally assigned on the basis of theoretical considerations while we measured 1876 lines. The treatment of the 1.58 μm transparency window corresponding to the lowest energy bands of the icosad is particularly challenging. Very recently, Nikitin et al. have succeeded in assigning and reproducing about 2000 transitions of our LNT and RT line lists near 6350 cm^{-1} [14]. Although limited to the $5\nu_4$ and $\nu_2+4\nu_4$ band systems of the main isotopologue and even if the data reproduction could not reach the experimental accuracy, the developed effective Hamiltonian approach [14] provided highly valuable information such as the accurate band centers of the eight $5\nu_4$ sublevels. In the few cases where the theoretical model predicts several coinciding transitions which were considered as a single line in the line profile fitting of the CRDS spectrum, the single experimental line may be replaced by the several components predicted by the model with the same (experimental) position and the empirical line intensity distributed according to the predicted relative intensities. Although suitable to take advantage of the recent theoretical advances, the proposed improvements (which represent

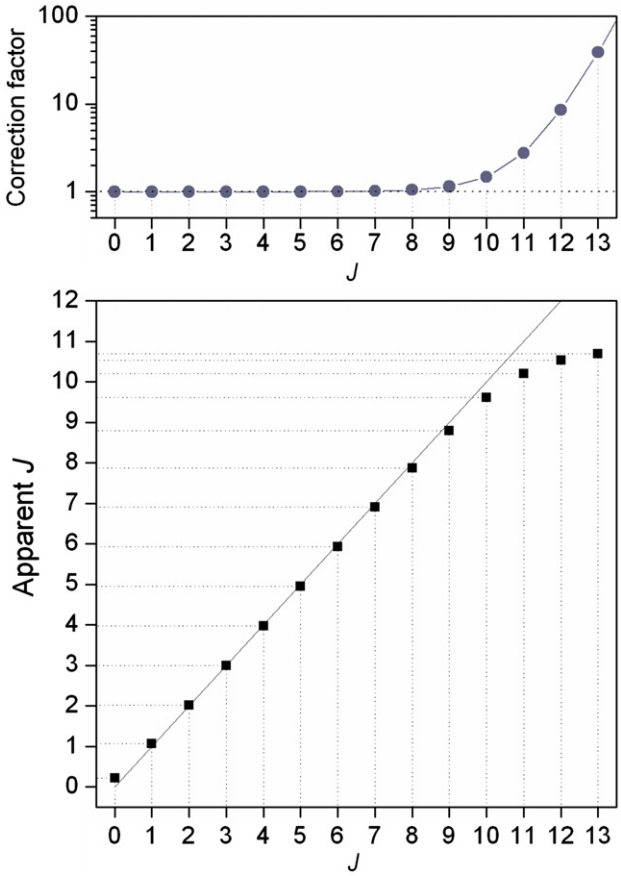

Fig. 12. Calculated impact on the measured absorption and empirical *J*-values of temperature gradient between the end of the cryostat and the super mirrors. *Upper panel:* ratio of the measured line intensity to the intensity value corresponding to a cell at a homogeneous temperature (80 K). Note the logarithmic scale adopted for the ratios. *Lower panel:* variation of the empirical *J*-values obtained neglecting the temperature gradient versus the actual *J*-values. The temperature gradient has no effect for *J*-values lower than 10.

a difficult and laborious task) are expected to lead to marginal changes for most applications.

Note that in Ref. [14], we have compared the rounded empirical *J*-values of the lower state with their theoretical values for the 836 lines whose calculated and measured line centers differ by less than 5×10^{-3} cm^{-1}. We obtained an agreement for 87% of the transitions, which illustrates the reliability of the "two-temperature" method.

7. Conclusion

The temperature dependence of the methane spectrum in the 1.58 μm transparency window of methane has been determined by applying the two-temperature method to CRDS spectra recorded at 80 K and room temperature. This experimental approach has the advantage of completeness, i.e. of providing spectroscopic information about the three isotopologues contributing to the spectrum of methane in "natural" abundance ($^{12}CH_4$, CH_3D and $^{13}CH_4$). The two-temperature method has proved to be a pragmatic approach fulfilling urgent needs in planetary science while the complete theoretical treatment of the spectrum of these three species is out of reach in the near future. In Fig. 14 we present a comparison of the total absorption to a low-resolution simulation of the absorption corresponding to the transitions for which the lower-state energy could be derived. Over the whole spectral region, the temperature dependence has been characterized for most of the absorption. Nevertheless, Fig. 8 shows that substantial improvements are still needed to identify the weak CH_3D transitions and determine their temperature dependence. As discussed in Section 3, the recent rovibrational assignments of the CH_3D spectrum at 80 K reported by Ulenikov et al. [26] are too limited (240 transitions) compared to the 1572 CH_3D transitions in our 80 K list. Improvements are particular needed near 6250 cm^{-1} where CH_3D is the main absorber at LNT. For this purpose, we are planning to use DAS to record new CH_3D spectra with an increased sensitivity both at RT and LNT.

The Wang-Kassi-Campargue (WKC) line list at 80 K attached as Supplementary Material is of particular importance for the studies of the giant planets and Titan. For instance, the methane absorption in the considered transparency window is so weak that observations of Titan allow probing the lower atmospheric levels (troposphere) and all the way down to the surface [35,36]. Our line list has the advantage to correspond to CH_3D abundance and temperature conditions which are close to those existing in the Titan

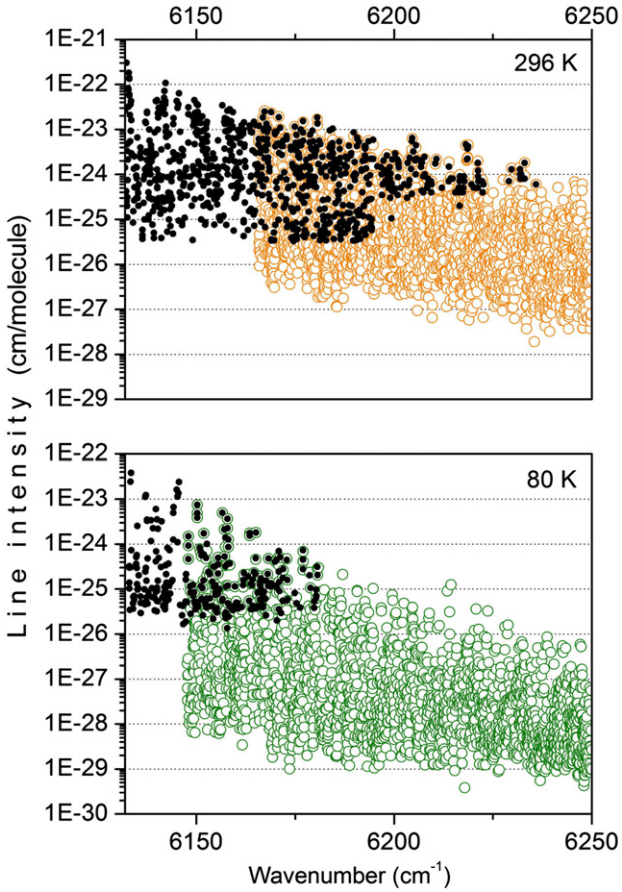

Fig. 13. Overview comparison of different line lists in the 6140–6250 cm^{-1} region corresponding to the high energy part of the tetradecad. *Upper panel:* Room temperature. The GOSAT line list (full circles) is presented superimposed to the CRDS line list [1]. *Lower panel*: Low temperature (80 K). The line list obtained by direct absorption spectroscopy [10] (full circles) is presented superimposed to our CRDS line list.

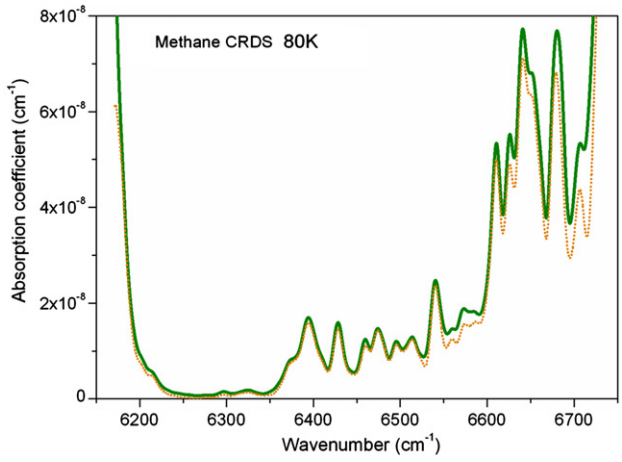

Fig. 14. Part of the methane absorption at 80 K for which the temperature dependence has been derived in the 6150–6750 cm^{-1} region. The solid line corresponds to a low resolution simulation (FWHM = 10.0 cm^{-1}) of the methane spectrum at 80 K and 1 Torr while the dashed line corresponds to a similar simulation limited to the lines with lower-state energy derived by the "two-temperature" method.

atmosphere and thus to limit the extrapolation of the line intensities needed for the radiative transfer models. The present WKC-80K line list has already been compared with the various band models used so far in the analysis of planetary spectra and significant deviations were evidenced [37]. It was also used to account for the 6200–6600 cm^{-1}

region of Titan spectra recorded by FTS with the 4 m telescope of Kitt Peak National Observatory at a resolution of 1.2 cm^{-1}. It led to an excellent match of all CH_4 and CH_3D features and allowed a new derivation of the CH_3D/CH_4 and CO mole fractions on Titan [37].

In the future, planetary applications of the WKC-80K line list would include analysis (or re-analysis) of other objects with atmospheres containing methane, from giant planets (Uranus, Neptune) to exoplanets.

Acknowledgements

This work is part of the ANR project CH4@Titan (ref: BLAN08-2_321467) which is a joint effort among four French laboratories (ICB-Dijon, GSMA-Reims, LSP-Grenoble and LESIA-Meudon) to adequately model the methane opacity. The support of the Groupement de Recherche International SAMIA between CNRS (France), RFBR (Russia) and CAS (China) is acknowledged.

Appendix A. Supporting information

Supplementary data associated with this article can be found in the online version at doi:10.1016/j.jqsrt.2010.11.015.

References

[1] Campargue A, Wang L, Liu AW, Hu SM, Kassi S. Empirical line parameters of methane in the 1.63–1.48 μm transparency window by high sensitivity Cavity Ring Down Spectroscopy. Chem Phys 2010;373:203–10.
[2] Liu AW, Kassi S, Campargue A. High sensitivity CW-cavity ring down spectroscopy of CH_4 in the 1.55 μm transparency window. Chem Phys Lett 2007;447:16–20.
[3] Rothman LS, Gordon IE, Barbe A, Benner DC, Bernath PF, Birk M, Boudon V, Brown LR, Campargue A, et al. The HITRAN 2008 molecular spectroscopic database. J Quant Spectrosc Radiat Transfer 2009;110:533–72.
[4] Kassi S, Romanini D, Campargue A. Mode by Mode CW-CRDS at 80 K: application to the 1.58 μm transparency window of CH_4. Chem Phys Lett 2009;477:17–21.
[5] Wang L, Kassi S, Liu AW, Hu SM, Campargue A. High sensitivity absorption spectroscopy of methane at 80 K in the 1.58 μm transparency window: Temperature dependence and importance of the CH_3D contribution. J Mol Spectrosc 2010;261:41–52.
[6] Kassi S, Gao B, Romanini D, Campargue A. The near infrared (1.30–1.70 μm) absorption spectrum of methane down to 77 K. Phys Chem Chem Phys 2008;10:4410–9.
[7] Gao B, Kassi S, Campargue A. Empirical low energy values for methane transitions in the 5852–6181 cm^{-1} region by absorption spectroscopy at 81 K. J Mol Spectrosc 2009;253:55–63.
[8] Sciamma-O'Brien E, Kassi S, Gao B, Campargue A. Experimental low energy values of CH_4 transitions near 1.33 μm by absorption spectroscopy at 81 K. J Quant Spectrosc Radiat Transfer 2009;110:951–63.
[9] Campargue A, Wang L, Kassi S, Mašát M, Votava O. Temperature dependence of the absorption spectrum of CH_4 by high resolution spectroscopy at 81 K: (II) The Icosad region (1.49–1.30 μm). J Quant Spectrosc Radiat Transfer 2010;111:1141–51.
[10] Wang L, Kassi S, Campargue A. Temperature dependence of the absorption spectrum of CH_4 by high resolution spectroscopy at 81 K: (I) The region of the $2\nu_3$ band at 1.66 μm. J Quant Spectrosc Radiat Transfer 2010;111:1130–40.
[11] Votava O, Mašát M, Pracna P, Kassi S, Campargue A. Accurate determination of low state rotational quantum numbers ($J < 4$) from planar-jet and liquid nitrogen cell absorption spectra of methane near 1.4 micron. Phys Chem Chem Phys 2010;12:3145–55.
[12] Sowers T. Late Quaternary Atmospheric CH_4 Isotope record suggests Marine clathrates are stable. Science 2006;311:838–40.
[13] de Bergh C, Lutz BL, Owen T, Maillard JP. Monodeuterated methane in the outer solar system. IV. Its detection and abundance on Neptune. Astrophys J 1990;355:661–6.
[14] Nikitin AV, Thomas X, Régalia L, Daumont L, Von der Heyden P, VlG Tyuterev, Wang L, Kassi S, Campargue A. Assignment of the $5\nu_4$ and $\nu_2+4\nu_4$ band systems of $^{12}CH_4$ in the 6287–6550 cm^{-1} region. J Quant Spectrosc Radiat Transfer 2011;112:28–40.
[15] Daumont L, Vander Auwera J, Teffo JL, Perevalov VI, Tashkun SA. Line intensity measurements in $^{14}N_2^{16}O$ and their treatment using the effective dipole moment approach: I. The 4300–5200 cm^{-1} Region. J Mol Spectrosc 2001;208:281–91.
[16] Ménard-Bourcin F, Ménard J, Boursier C. Temperature dependence of rotational relaxation of methane in the $2\nu_3$ vibrational state by self- and nitrogen-collisions and comparison with line broadening measurements. J Mol Spectrosc 2007;242:55–63.
[17] de Bergh C, Lutz BL, Owen T, Brault J, Chauville J. Monodeuterated methane in the outer solar system. II. Its detection on Uranus at 1.6μm. Astrophys J 1986;311:501–10.
[18] de Bergh C, Lutz BL, Owen T, Chauville J. Monodeuterated methane in the outer solar system III. Its abundance on Titan. Astrophys J 1988;329:951–5.
[19] Penteado PF, Griffith CA, Greathouse TK, de Bergh C. Measurements of CH_3D and CH_4 in Titan from infrared spectroscopy. Astrophys J 2005;629:L53–6.
[20] Lutz BL, de Bergh C, Maillard JP. Monodeuterated methane in the outer solar system. I. Spectroscopic analysis of the bands at 1.55 and 1.95 μm. Astrophys J 1983;273:397–409.
[21] Boussin C, Lutz BL, de Bergh C, Hamdouni A. Line intensities and self-broadening coefficients for the $3\nu_2$ band of monodeutrated methane. J Quant Spectrosc Radiat Transfer 1998;60:501–14.
[22] Boussin C, Lutz BL, Hamdouni A, de Bergh C. Pressure broadening and shift coefficients for H_2, He and N_2 in the $3\nu_2$ band of $^{12}CH_3D$ retrieved by a multispectrum fitting technique. J Quant Spectrosc Radiat Transfer 1999;63:49–84.
[23] Coustenis A, Achterberg R, Conrath B, Jennings D, Marten A, Gautier D, Nixon C, Flasar F, Teanby N, et al. The composition of Titan's stratosphere from Cassini/CIRS mid-infrared spectra. Icarus 2007; 189:35–62.
[24] Penteado PF, Griffith CA. Ground-based measurements of the methane distribution on Titan. Icarus 2010;206:345–51.
[25] Bézard B, Nixon CA, Kleiner I, Jennings DE. Detection of $^{13}CH_3D$ on Titan. Icarus 2007;91:397–400.
[26] Ulenikov ON, Bekhtereva ES, Albert S, Bauerecker S, Hollenstein H, Quack M. High resolution infrared spectroscopy and global vibrational analysis for the CH_3D and CHD_3 isotopomers of methane. Mol Phys 2010;108:1209–40.
[27] Nikitin AV, Mikhailenko S, Morino I, Yokota T, Kumazawa R, Watanabe T. Isotopic substitution shifts in methane and vibrational band assignment in the 5560–6200 cm^{-1} region. J Quant Spectrosc Radiat Transfer 2009;110:964–73.
[28] Margolis JS. Empirical values of the ground-state energies for methane transitions between 5500 and 6150 cm^{-1}. Appl Opt 1990;29:2295–302.
[29] Pierre G, Hilico JC, de Bergh C. The region of the $3\nu_3$ band of methane. J Mol Spectrosc 1980;82:379–93.
[30] Champion JP, Hilico JC, Brown LR. The vibrational ground state of $^{12}CH_4$ and $^{13}CH_4$. J Mol Spectrosc 1989;133:244–55.
[31] 〈http://gosat.nies.go.jp〉.
[32] Nikitin AV, Lyulin OM, Mikhailenko SN, Perevalov VI, Filippov NN, Grigoriev IM, et al. GOSAT-2009 methane spectral linelist in the 5550–6236 cm^{-1} range. J Quant Spectrosc Radiat Transfer 2010; 111:2211–24.
[33] Margolis JS. Measured line positions and strengths of methane from 5500 to 6180 cm^{-1}. Appl Opt 1988;27:4038–51.
[34] Brown LR. Empirical line parameters of methane from 1.1 to 2.1 μm. J Quant Spectrosc Radiat Transfer 2005;96:251–70.
[35] Griffith CA, Owen T, Wagener R. Titan's surface and troposphere, investigated with ground-based, near-infrared observations. Icarus 1991;93:362–78.
[36] Tomasko MG, Smith PH. Photometry and polarimetry of Titan - Pioneer 11 observations and their implications for aerosol properties. Icarus 1982;51:65–95.
[37] de Bergh C, Courtin R, Bézard B, Coustenis C, Lellouch E, Hirtzig M, Drossart P, Campargue A, Kassi S, Le Wang, Boudon V, Nikitin A, Tyuterev V. Implications of a new CH_4 database on the analysis of Titan spectra in the 1.56 μm window. Plan Space Sci 2010 submitted.